DOI: 10.15201/hungeobull.73.4.3 Hungarian Geographical Bulletin **73** 2024 (4) 379–394.

GIS and soil property-based development of runoff modelling to assess the capacity of urban drainage systems for flash floods

András DOBAI[1], András HEGEDŰS[1], János VÁGÓ[1], Károly Zoltán KOVÁCS[1], Anna SERES[1], Péter PECSMÁNY[1] and Endre DOBOS[1]

Abstract

The extreme precipitation resulting from climate change has been causing increasingly serious damage in populated areas over the past 10–15 years. The torrents of flash floods cause significant financial damage to both the natural environment and man-made structures (such as roads and bridges). The determination of the physical geographic parameters of this phenomenon (e.g. the amount of runoff water) is significantly affected by technical uncertainties, usually due to the lack of monitoring systems. However, the application of modern geospatial tools can improve the quality of input data needed for runoff modelling. In the present study, an existing runoff model (the Stowe model) developed by ESRI was further enhanced with field measurements, soil parameters, GIS, and remote sensing data, resulting in the creation of the model named ME-Hydrograph. Finally, the two models were compared, and we examined the capacity of an urban stormwater drainage system through surface runoff modelling. The aim of the research was to create a runoff model that can be easily and quickly used. The application of this geospatial model presented in the study can be useful not only in the examination of urban stormwater drainage but also in contributing to the understanding and management of flash floods that occur in Hungary. Additionally, it can aid in the development of risk mapping related to flash floods in the country.

Keywords: soil properties, GIS, flash flood, runoff modelling

Received July 2024, accepted December 2024.

Introduction

The increasing number of extreme precipitation events causing flash floods has posed a significant impact on various technical and scientific fields (flood management, hydrology, soil science etc.). Research related to this phenomenon has played a prominent role in recent years, particularly in the regarding of monitoring systems, valley characteristics, soil surface coverage and modelling the recession of flood waves and climate trends (Guo, L. *et al.* 2018, Jakab, G. *et al.* 2019; Du, J. *et al.* 2020; Ramos Filho, G.M. *et al.* 2021; Víg, B. *et al.* 2022; Mikes, M.Z. *et al.* 2024). The stormwater flow velocity depends on factors such as land cover and surface roughness, as different terrain features influence velocity to varying degrees (Agroszkin, I.I. *et al.* 1952; Chow, V.T. 1959). The analysis and incorporation of these additional factors into runoff modelling were first achieved with the 1995 release of HEC-RAS and HEC-HMS (Hydrologic Engineering Center's River Analysis System and Hydrologic Modelling System); however, these programs require significant input data.

In the examination of flood waves occurring in Hungary, flood wave characterization was first achieved through a detailed analysis of the accumulation-runoff process in areas where no representative water gauge station or cross-section of a watercourse was present. The resulting methods have continuously been expanded and evolved with

[1] Institute of Geography and Geoinformatics, Faculty of Earth- and Environmental Science and Engineering, University of Miskolc. Egyetemváros, HU-3515 Miskolc, Hungary. Corresponding author's e-mail: andras.dobai@uni-miskolc.hu

other surface data (catchment characteristics and soil properties) provided by geography (Pirkhoffer, E. *et al.* 2013; Koris, K. 2021). With the development of GIS and remote sensing methods, modelling opportunities have expanded through the numerical processing of these data. However, when such extreme precipitation events (precipitation intensity above 35 mm/h (Goda, Z. 2019) are reconstructed, limitations may arise (Czigány, Sz. *et al.* 2009). Furthermore, mapping methodologies for flash flood risks are still under development due to deficiencies in the spatial resolution of hydrological and soil databases. Researchers lack data on small catchment areas surrounding settlements, as well as their runoff characteristics, and the intensity of precipitation events can vary.

The basis for designing urban stormwater drainage structures relies on methods applied in technical hydrology. However, these methods often involve approximate estimates due to the lack of incoming data (Kontur, I. *et al.* 2003). Quantitative data that provide greater technical safety, such as mapping and field assumptions (e.g. Lidar DEM, soil sampling, and laboratory analysis), are associated with significant costs. With the advancement of geospatial tools, these estimates can be optimized and improved using interdisciplinary methods. Beyond describing surface properties (slope steepness, topological wetness index, valley density, etc.), it is crucial to provide the most reliable data on the expected flood wave characteristics with minimal input data and uncertainty.

In this study, we present an assessment of the capacity of a stormwater drainage network in a settlement vulnerable to flash floods. The study goal was to develop a GIS tool for modelling surface runoff and infiltration processes for water falling on the urban surface and flowing in from the external parts of the catchment. The modelling utilized data on topography, land use, built environment, and soil conditions, supplemented with parameters from the technical description of the drainage system provided by civil engineers. The GIS-based simulation was implemented in the ESRI ArcGIS 10.1 environment. The input layers used for running the model were organized into a GIS database. Since the surface runoff-infiltration characteristics are fundamentally determined by the soils in the sample area, their physical properties and further parameters were investigated through field measurements at representative locations. To facilitate and expedite the iterative runs of the modelling, we developed a Python-based tool capable of calculating and analyzing water yields. The results of the model runs were ultimately compared with the capacity data from the technical plan documentation of the drainage system. The advantage of the model is that data are provided with high reliability despite relatively small field data sampling.

Study area

The study area is located in the eastern part of the Nyögő-Harica catchment, near the border of Sajószentpéter, in Northern Hungary *(Figure 1).* A significant portion of the catchment is situated in the northern foothills of the Bükk Mountains, in the Tardona Hills, extending into the Northern Bükk in the west, while its north-eastern part is bordered by the Sajó Valley.

Geologically, the area is located in the East-Borsod Coal Basin. The basin is composed of alternating layers of Neogene marine and lacustrine sediments of various ages, along with Miocene pyroclastics, often deposited with erosional discordance (Kozák, M. and Püspöki, Z. 1995; Kozák, M. *et al.* 1998; Harangi, Sz. 2001). Most Quaternary sediments are products of weathering from the aforementioned rocks. Due to sequential tectonic processes during the Miocene to Quaternary, the area has been fragmented in a mosaic pattern (Kozák, M. and Püspöki, Z. 1995; Pelikán, P. 2002). The area's topography is fundamentally shaped by these geological and structural characteristics (Sütő, L. 2001). The erosion rate is significant in the area, with a valley density of ~ 3.0 km/km^2 (Baros, Z. *et al.* 2001), and an average stream density in the hilly region of 2.7 km/km^2. The average relative

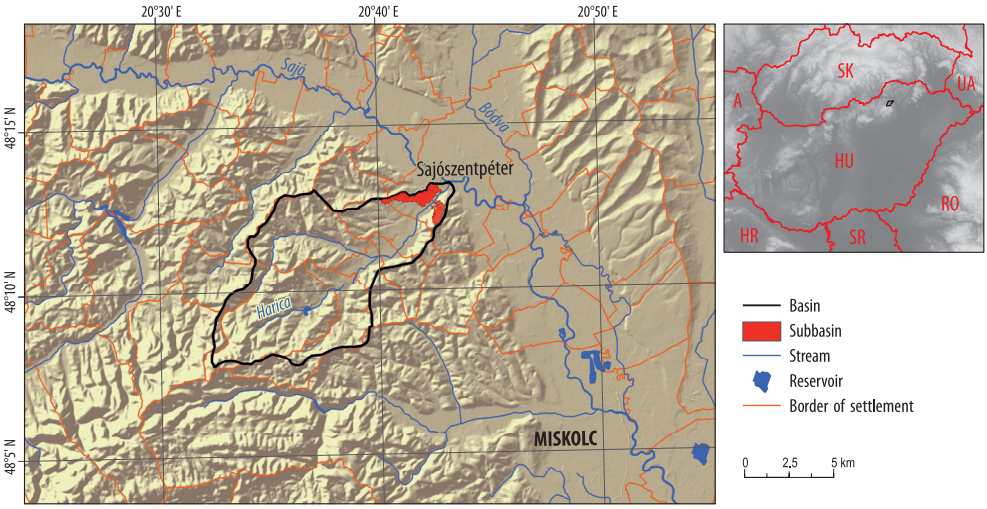

Fig. 1. Location of the study area. *Source:* Elaborated by the authors.

relief is 105 m/km², while in areas bordering the Sajó Valley, it is 80 m/km² (Dövényi, Z. 2010). The examined area has a moderately warm to moderately dry climate (Bihari, Z. *et al.* 2018), becoming moderately warm and dry around 2050 (Bihari, Z. *et al.* 2018). The annual mean temperature varies from 8.8–9.3 °C. The average maximum temperature on the warmest summer days is 31–33 °C, while the average minimum temperature on the coldest winter days is -17 °C. The annual precipitation ranges from 550 to 600 mm. The prevailing wind directions are northwest and northeast, aligning with the topography, and the average wind speed is 2.5 m/s (Péczely, Gy. 2006; Dövényi, Z. 2010). Within the study area, the main determinants of soil diversity are the parent rock and topography. In the Harica Valley Gleysols (Aqualfs) with heavy clays have developed. The northern watershed areas are covered by Stagnic Luvisols (Epiaqualfs). Areas of higher elevation are covered by loess-like, physically heterogeneous sediments, on which area Luvisols (Alfisol) have developed. The southern watershed areas are covered by eroded Arenosols (Psamments), Arenic Phaeozems (Haplustolls), and Leptosols (Lithic Alfisols) *(Figure 2).*

More than half of the Tardona Hills is covered by grass vegetation, while nearly a quarter is covered by forests. Human activity extensively transformed vegetation during the medieval period, leading to the fragmentation of forest communities. The grasslands are mainly composed of patches of fescue (*Festuca*), reed bentgrass (*Calamagrostis epigeios*), and false brome (*Brachypodium sp*). The predominant forest communities include Turkey oak forest (*Quercetum petraeae-cerris*, covering 43% of the forests) and the hornbeam-oak forest (*Caricipilosae-Carpinetum*, covering 33% of the forests) in higher regions. The proportion of forest patches composed of invasive species is considered low, with notable ones being the black locust stands (8.6% of forests) and the Norway spruce forests (*Picea abies*, 1.7% of forests) (Szirmai, O. and Czóbel, Sz. 2008).

Based on the Flood Calculation Guide issued by the General Directorate of Water Management of Hungary, the flood discharges calculated for the study area at the firth of Nyögő Stream, with a specific discharge of Q_5% m³/s km², are as follows: Q_1% = 71.0 m³/s, Q_3% = 54.6 m³/s, Q_{10}% = 38.2 m³/s (Koris, K. 2021). However, these values refer to the entire catchment area, not to the small

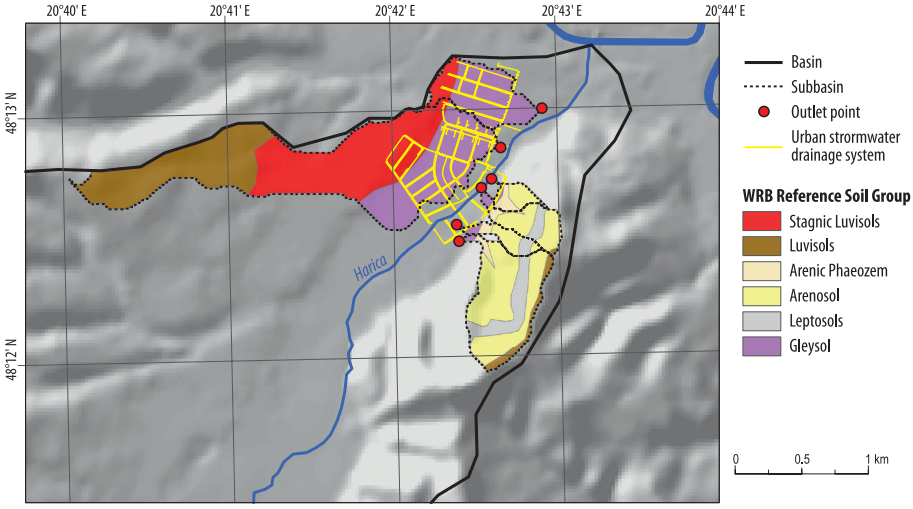

Fig. 2. Digital soil map of the study area. *Source:* Elaborated by the authors.

catchments surrounding the settlement. The Flood Calculation Guide cannot be applied to catchments smaller than 2 km² or can only be applied if there is thorough knowledge of the catchment area and the use of the so-called hydrological analogy. Therefore, new methods should be sought using GIS and remote sensing data to study catchments that are still hydrologically unexplored.

Materials and methods

Introduction of Stowe-Hydrology tool

As the first step in the research, the selection of a runoff model was necessary, with criteria requiring it to be freely accessible and user-friendly. This led to the selection of the Stowe-Hydrology model developed by ESRI (arcgis.com). The Stowe model utilizes slope steepness, flow direction, and accumulation grids derived from a digital elevation model (DEM), along with watershed boundaries and outlet points, as input data to determine runoff velocity. In this way, a general overview of surface runoff can be obtained.

Determining the runoff requires knowledge of the quantity of flowing water, as well as the size of watershed area and runoff time also. For this purpose, the runoff velocity needs to be determined using the method proposed by Maidment, D.R. *et al.* (1996). While this method accounts for spatial variability in runoff velocity, it ignores temporal changes and recession of precipitation and the amount of runoff water. In real scenarios, runoff velocity changes over time, influenced by the rate of recession. According to our current level of technical knowledge, this dynamic change is difficult to model, allowing us to obtain only a general picture of the problem. Nevertheless, it can be considered suitable for modelling larger floods (e.g. precipitation intensity above 35 mm/h), as studies conducted in Australia found that runoff velocity remains relatively constant during major floods (Pilgrim, D.H. 1976). During calculation, each pixel in the elevation model receives a velocity value based on the slope of the terrain it covers and the size of the watershed area above it. This is determined by the following equation (Eq 1, Flow Accumulation).

$$V = V_m \cdot \frac{S_b^{\cdot} A_c}{s^b A_m^c}, \qquad (1)$$

where: V is the runoff velocity associated with the pixel of interest; V_m is the average runoff velocity characteristic to the watershed area. We assume a runoff velocity of 0.1 m/s based on Maidment, D.R. *et al.* (1996); s is the slope of the area covered by the pixel; A is the size of the contributing area to the pixel, where water is directed (Flow Accumulation); b and c are empirical exponents, which Maidment, D.R. *et al.* (1996) defined as 0.5 for similar types of areas; $s^bA^c{}_m$ is the average slope-to-watershed ratio.

The model cuts unrealistically high or low velocity values (above 2 m/s or below 0.02 m/s) and equates them to threshold values. The runoff time represents the time it takes for water to reach a specific point from the furthest point in the watershed. For the study, we used the weighted option of the ArcMap Flow Length tool. The weighting factor indicates how much time the water needs to pass through a cell. In this case, this time, in line with the above, can be calculated as the reciprocal of the velocity, 1/v, since the greater the velocity, the less time the runoff water spends on a cell. After classifying the runoff velocity, an isochrone map is generated, which provides the Unit Hydrograph (UH) to depict the surface runoff wave produced by a unit of precipitation. The hydrograph enables analysis of the intensity and temporal distribution of runoff caused by precipitation events (Maidment, D.R. *et al.* 1996).

The Stowe model does not consider precipitation intensity, land cover, surface infiltration, and storage conditions, also it can handle only one watershed at a time. Our model was developed using these input data, and a comparison was made between the two models.

Introduction of ME-Hydrograph model

We enhanced the model by developing a separate tool in Python called ME-Hydrograph, making it suitable for integration into the ArcGIS Toolbox. The new simulation model for stormwater runoff relies on numerous additional input data for calculating hydrological processes. These include precipitation data from recent years, topographical characteristics determining accumulation, spatial extent and ratio of impervious and pervious surfaces, as well as the physical properties of various soil types, especially soil saturation conditions and infiltration factors.

The new model was applied in the study of the stormwater drainage system load in the town of Sajószentpéter. The input data used were as follows: a DEM with a spatial resolution of 5 metres, precipitation data from the nearest meteorological station, Sentinel multispectral satellite images for land use mapping, as well as literature-based soil type data, surface coverage, and in-situ measured soil infiltration and saturation values extended based on field knowledge and surveys. The drainage network was designed by selecting valleys of Harica Stream that terminate in the sewage system of Sajószentpéter. Subsequently, points were chosen where these valleys join the stream. For precise alignment, we "snapped" these points to the theoretical water flow network (Snap Pour Point), and then used the Watershed command to calculate the sub-watersheds corresponding to the respective outlets. In the area, six sub-watersheds were identified from which water drains into the city's drainage network. We analysed in details the small watershed labeled as number 5. Additional parameters will be discussed in the following sections.

Mapping of topography and surface properties of the sample area

Based on the 5 m resolution digital elevation model, the delineation of the entire catchment area, as well as the Harica and Nyögő streams, was completed. For the land-use layer, Sentinel-2b multispectral satellite imagery with a resolution of 10 metres was used, captured on 27 September 2016. The utilized channels were B2 (blue), B3 (green), B4 (red), B8 (NIR), and the 10-metre resam-

pled B5 (VNIR). Training areas were established for the classification of individual pixels in satellite images, which were identified through a combination of field surveys and aerial photographs captured simultaneously with higher spatial resolution. The classification was performed using MultiSpec software (https://engineering.purdue.edu/~biehl/MultiSpec/), creating eight land-use categories with supervised classification.

Integration of precipitation conditions into the model

Since there is no regular precipitation measurement in Sajószentpéter, the precipitation data used for running the simulation model are derived from measurements at the nearest (Putnok) meteorological station based on Hungarian Meteorological Service database also the annual hydrometeorological reports from the General Directorate of Water Management of Hungary were further utilized *(Table 1)*. Since 2010, extreme precipitation events have been recorded almost annually in the region, leading to the development of mesoscale convective system (MCS) storms that generate flash floods. These storms are predominantly observed between April-May until October, but typically develop most frequently during the summer months.

Mapping of soil properties of the sample area

The purpose of the soil survey was to provide input data based on real measurements and field experiences. The soil diversity within the watershed significantly influences the surface runoff of precipitation. A portion of the precipitation infiltrates into the soil and then, after the soil is saturated, begins to flow on the surface. To quantify this phenomenon, we measured the soil infiltration rate at five locations using a ring infiltrometer, and soil profiles were also excavated, and soil samples were sent to laboratory for analyses. The main purpose of the "constant head" method used to measure the amount of water infiltrating into the soil per unit of time is to place two metal frames into the top 30 cm of soil. The outer frame provides constant hydrostatic pressure to ensure that the water in the inner frame infiltrates deeper into the soil and does not escape laterally (Várallyay, Gy. and Fórizs, J. 1966).

During the infiltration test we examined how land cover, especially traditional agricultural cultivation, affects the structure of soils, influencing their water-conducting and water-retaining capacities. At sampling sites 1 and 2, where the frames were placed 40 metres apart on the same soil type but under different cultivation intensities, the infiltra-

Table 1. Daily precipitation totals during MCS stroms

Date	Precipitation amount, mm/24 h	Date	Precipitation amount, mm/24 h
06.05.2010	34.2	22.10.2014	34
15.05.2010	60.4	17.08.2015	33
16.05.2010	37.2	19.08.2015	42.5
25.07.2010	33.2	13.07.2016	35.2
09.06.2011	94	10.06.2018	49.2
29.07.2012	36.4	23.05.2019	32
24.06.2013	59.6	23.06.2019	91.3
15.10.2013	40.2	13.08.2019	76.8
04.08.2014	32.2	26.06.2020	57.2
10.09.2014	46.7	13.10.2020	46.8

Source: Hungarian Meteorological Service.

tion was practically zero in conventionally tilled fields. In less compacted fields with roots, two orders of magnitude greater infiltration that significantly dampened precipitation events were measured. At sampling sites 3 and 4, the drastic difference in permeability was also influenced by the cultivation technology applied in the area. In the case of meadows, due to the cracks in the marshy soil and the dense root system of soft-stemmed plants, precipitation immediately infiltrates into the deeper layers of the soil, while in the cultivated seedbed, the natural cracking of the soil is worked out, and the drainage capacity is almost zero. This effect is periodic: during wet periods, the soil of the meadow swells with moisture and, similar to the seedbed, it seals. The infiltration data measured at sampling site 5 show that a significant portion of the precipitation infiltrates due to the good water-conducting properties of the soil's coarse physical nature, indicating that the method well reflects the soil's physical nature.

The vegetation improves the soil's water-conducting capacity mainly through its root network, thereby acting as a brake on surface runoff. In the case of forest vegetation, the canopy also retains a significant amount of water before it reaches the soil (Balatonyi, L. 2015). For steep terrain, the amount of precipitation falling in windless weather on a unit area is also less. These results were taken into account in the spatial extension, and the land cover map also explains the variability of the results.

Results and discussion

Results of the model input parameters

The results of land use mapping from the Sentinel 2 satellite imagery are as follows *(Figure 3).* During the supervised classification 8 classes (arable, forest, built-up, etc.) were created, during classification an average accuracy of 98.5 percent and a kappa accuracy value of 97.0 percent were achieved, which metric demonstrates that the individual land cover classes are perfectly separated within the classification model.

The built-up, covered areas account for 3.57 percent of the analyzed catchment, while the uncovered, infiltrating areas make up 96.43 percent. The proportions of the land-use classes obtained from the classification results are summarized in *Table 2*.

Distinct infiltration and runoff characteristics are exhibited by the individual land cover classes. Therefore, the most representative roughness coefficients were assigned to each class: forest = 0.3; pasture = 0.6; arable land = 0.8; built-up area = 1. In the model, by multiplying the velocity with this land cover raster, we obtained the area-specific modified flow velocity. During the modelling process, the previously presented extreme precipitation intensities (see *Table 1*) were utilized as input data, and the individual scenarios were tested. Comparisons were made with the Stowe model, the results of which are discussed in a subsequent chapter.

Results of input soil parameter analysis

Field and laboratory soil measurements are crucial for determining the model input soil parameters and their spatial extension. Laboratory analyses of the samples focused on essential soil physics parameters for accurate parameterization of the hydrological model (soil mechanics, bulk density, etc.). The soil's physical heterogeneity varies with the topography. The occurrence of loose sediments in the area can be linked to the topographic situation. Therefore, when creating maps of physical heterogeneity, the digital elevation model (DEM) and the geological map as auxiliary variables for spatial extension (Universal Co-Kriging interpolation) were used. As the pore conditions and water retention capacity depend strongly on land use, these data were used when creating maps of pore space and measured water drainage capacity. In the temporal modelling of rainfall runoff, we considered pore space and infiltration speed and modified the runoff speed based on land-

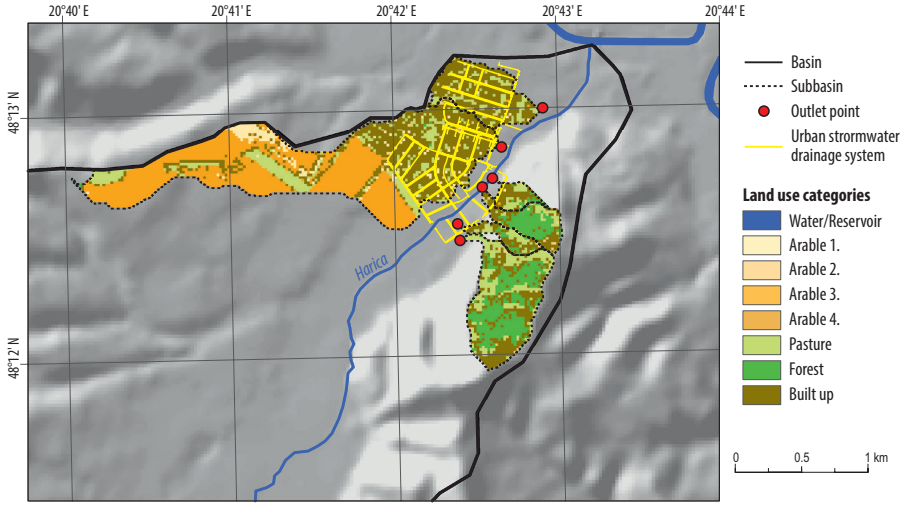

Fig. 3. Land-use map of Harica-Nyögő watershed. *Source:* Elaborated by the authors.

Table 2. Extent and percentage of land-use classes

Land use	Extent, km²	Class percentage, %
Water surface	0.1016	0.128084
Forest	46.9528	59.192060
Pasture	16.4388	20.723930
Arable land 1	0.6592	0.831035
Arable land 2	4.2716	5.385085
Arable land 3	0.2808	0.353997
Arable land 4	7.7824	9.811051
Built-up area	2.8356	3.574760
Total	*79.3228*	*100.000000*
Overall class perf., %	98.5	–
Kappa Statistic (X100), % Kappa Variance	97.0 0.000018	–
Av. likelihood prob., %	38.1.	–

use data. The saturation of the pore space varies depending on the precipitation intensity, the results of which are as follows *(Table 3)*.

Based on the data of the soils sampled and analyzed in the laboratory during the field survey *(Table 4)*, we first mapped the spatial distribution of soil particle sizes, a parameter that well characterizes pore conditions and, thus, water retention capacity.

During the ME-Hydrograph model run, the periodic differences in water saturation can also be considered and adjusted. For this purpose, infiltration rate and capacity values were calculated for the area based on field measurements, extended by the digital elevation model. When designing the model, we multiplied the soil's water absorption capacity by a saturation factor between 0 and 1, which indicates the soil's capacity to absorb water at a given moment. For example, summer-dried soil was assigned to a factor of 0.8, while a winter-frozen soil gets a fac-

Table 3. Results of infiltration measurements

Measure	Amount of water, mm	K_ AVG, mm/s	Infiltrate_ AVG, m	Infiltrate_time, min	Soil type	Land use	Position
Frame 1 (SSZTP_1)	170	0.04	0.08	85	Luvisol	arable land	mid-slope
Frame 2 (SSZTP_1)	180	0.02	0.02	83	Gleysol	arable land	plane
Frame 3 (SSZTP_2)	210	3.12	0.14	10	Luvisol	meadow	slope shoulder
Frame 4 (SSZTP_2)	205	0.01	0.05	136	Luvisol	arable land	slope shoulder
Frame 5 (SSZTP_3)	190	2.11	0.13	10	Luvisol	meadow	hilltop, shoulder

Note: SSZPT = Sajószentpéter.

Table 4. Results of soil sample analysis

Sample ID	Depths, cm	Sand%, 0.05–2 mm	Silt%, 0.002–0.05mm	Clay, < 0.002 mm
SSZTP01/1	0–10	36.7	24.5	38.9
SSZTP01/2	10–25	34.5	24.1	41.3
SSZTP01/3	25–40	33.7	21.8	44.5
SSZTP01/4	40–80	35.6	20.4	44
SSZTP01/5	80–100	36.6	20.7	42.7
SSZTP02/1	0–25	35.28	31.94	32.78
SSZTP02/2	30–50	25.51	25.75	48.74
SSZTP02/3	50–100	23.04	24.45	52.51
SSZTP03/1	0–10	73.29	13.41	13.30
SSZTP03/2	10–30	72.77	11.17	16.06
SSZTP03/3	30–50	86.45	5.37	8.18
SSZTP04/1	0–20	47.92	19.68	32.40
SSZTP04/2	20–55	39.35	20.63	40.02
SSZTP04/3	55–75	38.59	19.04	42.37
SSZTP04/4	75 <	38.97	18.50	42.53

tor of 0.1. In this way, the time it takes for the soil to reach saturation was calculated for each pixel.

If the soil cannot infiltrate because the infiltration rate is lower than the precipitation intensity, the excess appears as runoff discharge. Similarly to the Stowe-Hydrology tool, the time of concentration and velocity elements were integrated into the model as discussed earlier. Adding this time to the runoff time, we get how long it takes for water to flow from the pixel to the outlet point from the start of rainfall, depending on soil quality, land cover, slope, and watershed size. This modified runoff time raster was classified into 10-minute intervals for ease of subsequent calculations and overview *(Figure 4).*

This classified isochrone map shows how many pixels drain water to the outlet point

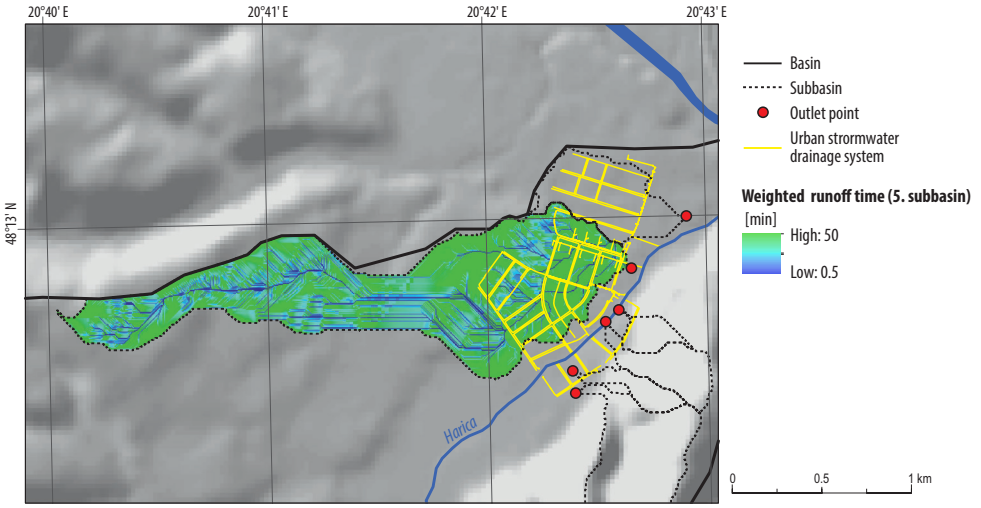

Fig. 4. Weighted runoff raster dataset for 5th outlet point. *Source:* Elaborated by the authors.

in a given 10-minute interval from the start of rainfall. For rainfall events lasting longer than 10 minutes, we had to add the areas of these 10-minute bands from the outlet point to the end of the rainfall duration. When the rain stops, we add any 10-minute bands remaining in the upper part of the watershed, as this water has not yet flowed. At the same time, we subtract the 10-minute bands located downstream, as this water has already left the area.

We then calculated the amounts of water that flowed through the outlet points and their associated times. We multiplied the pixel counts by the pixel area (25 m²) to obtain the areas in square metres for each 10-minute interval. By dividing the rainfall amount by the rainfall duration, we calculated the rainfall intensity, i.e., the rate of rainfall in mm per second. By graphing these data, we obtained hydrographs, which show how the quantity of water flowing through the outlet point changes over time for a given area, rainfall amount, and rainfall duration. As a result, a dataset weighted by surface properties and soil parameters (including porosity and infiltration rate) was generated and classified into 10-minute intervals *(Figure 5).*

Results of the comparison between the two runoff models

The outflow point 5, which forms the basis of the study, belongs to the largest watershed, covering an area of 1.4 km². Consequently, a scenario with 100 mm of precipitation over 240 minutes was examined for this watershed. The results of Stowe-Hydrology tool and ME-Hydrograph were compared (*Figure 6*), during which the peak values were multiplied by 100 to evaluate the discharge results provided by the two hydrographs.

In the hydrograph of the ESRI Stowe-Hydrology tool, it can be observed that at the 220th minute, a flow of 230 m²/s would reach the outflow point from the contributing area. The flood wave generated by the ME-Hydrogaph model, as shown in *Figure 6*, indicates that there is no significant discharge until the 230th minute because, up to that point, the soil has absorbed most of the water. Around the 230th minute, the curve starts to rise steeply and reaches its peak around the 350th minute when approximately 1700 l/s of water arrives at the discharge point. This delay occurs because it takes this amount of time for water from the upper

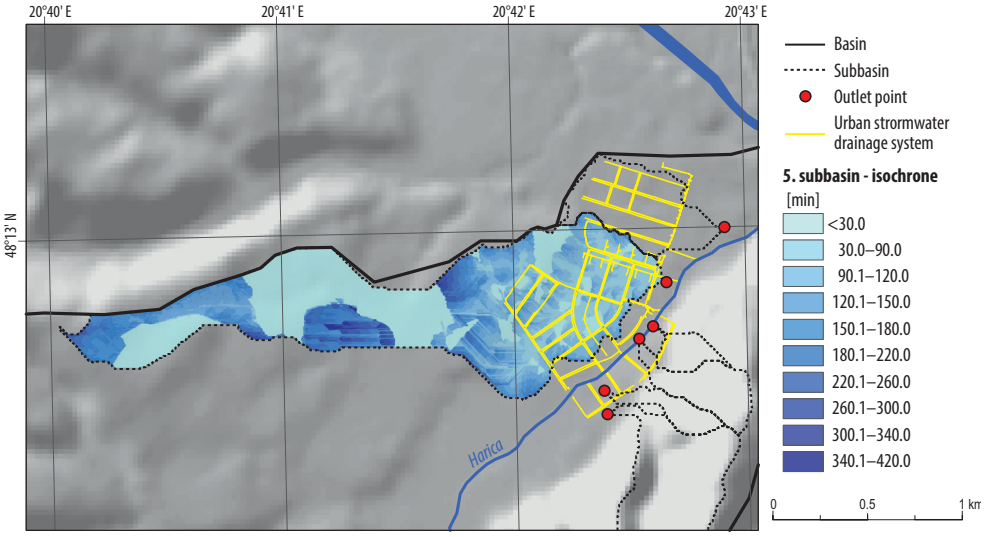

Fig. 5. 10-minute classified isochrone map of 5th outlet point (modified by surface cover and soil factors). *Source:* Elaborated by the authors.

parts of the watershed to reach the outlet. Along the descending branch of the curve, it can be observed that the water runoff from progressively smaller areas is completely exhausted after approximately 660 minutes.

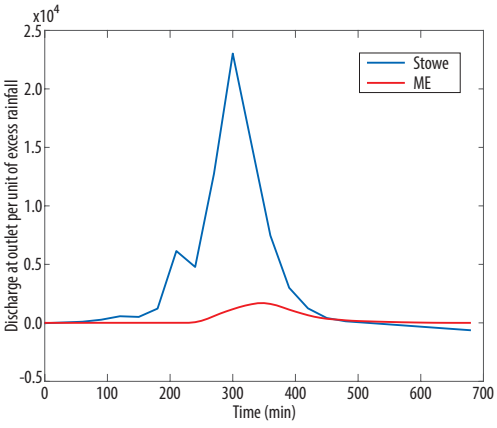

Fig. 6. Result of Simpson's 3/8 rule. *Source:* Elaborated by the authors.

The integration of the area under the two curves was performed using the Simpson's 3/8 method, which is a numerical integration procedure and a variation of Simpson's rule. The basic idea is to approximate the area under a given function using triples corresponding to the function values. The notation 3/8 indicates that the method uses three function values on each subinterval. The 3/8 method can provide more accurate results than the classical Simpson's rule, especially when the function values vary significantly within the integration range (Pandey, K. *et al.* 2011). The results obtained from the traditional trapezoidal integration method and the applied Simpson's rule were almost identical.

The areas under the curves show the amount of water that has flown through the outlet points. As the Y axis of the hydrograph (see *Figure 6*) has a unit of l/s, we have to convert that to l/min to be able to dismiss the min and get liter as the result of the integration of the curve. Thus, the above numbers were multiplied by 60 and then divided by 1000 to get the amount of water in m^3 (Eq 2, *Table 5*).

$$\text{Area under curve in m}^3 = \frac{\text{Integration of the area under curve} \cdot 60}{1000} \text{ [m}^3\text{]} \quad (2)$$

The area of the watershed is 1,383,975 m^2. The total amount of rain that has fallen to the area is calculated by multiplying the area of the watershed with the amount of rain, resulting 138,398 m^3 (Eq 3).

$$\text{Total amount of rain} = \text{Watershed [m}^2\text{]} \cdot \text{Amount of rain [m] [m}^3\text{]} \quad (3)$$

One can see that from the total amount of rain (138,398 m^3), only 16,252 m^3 has left through the outlet point, which is 11.7487 percent of the total precipitation, and, thus, 88.2513 percent was retained by the soil *(Table 6)*.

We can see about the same percentage if we check the areas under the Stowe and the ME curves. We get 147,646 m^3 as the result of the integration of the Stowe curve and we already know the 16,252 m^3 from the integration of the ME curve. The differences in the results between the two models can be attributed to the soil parameters (infiltration rate, pore space etc.), highlighting the significant retention effect that the initial properties of the soil have, particularly during the first hour of a precipitation event. As the Stowe model does not consider any infiltration, while the ME model does, the ratio between them should show the percentage that has been run off and retained. So, in this case 11.0074 percent of the water ran off and 88.9926 percent was retained by the soil (see *Table 6*). The reason the Stowe model does not match exactly with the total amount of precipitation calculated by the area · amount of precipitation, is that it uses some empirical constants.

The similarity of the percentages confirms that the GIS application developed by ME, models water runoff well by taking into account the water retaining capacity of the soil, thus, providing reliable hydrographs. Such consistency indicates that the method is robust and can yield results.

During the investigation, the model was also tested using rainfall events of varying intensities, with rainfall lasting half as long (50 mm/120 minutes) and twice as long (200 mm/480 minutes) as the previously presented intensity being analyzed. As a result of the first scenario, no water appeared at the outflow point because the water yield had been infiltrated by the soil. Under theoretical conditions of a 200 mm/480-minute rainfall event, around the 230th minute, a significant rise in outflow water was observed, and it was concluded that (similar to previous tests) around the 220th–230th minute, the soils had become saturated. It is important to note that these results strongly depend on the initial soil saturation. The aim of using the precipitation intensities presented in these examples was to validate the importance of initial soil parameters in runoff modelling.

Table 5. Result of Simpson's 3/8 method

Curves	Area under curve	
	from original hydrograph	in m^3 by Eq 2.
Stowe	2,460,772.1454	147,646.3287
ME	270,876.0551	16,252.5633

Table 6. Percentages of runoff and ratained water between the two models

Percentages	ME model/ Actual rain amount	ME model/ Stowe model
Runoff percent, %	11.7487	11.0074
Retained percent, %	88.2513	88.9926

Result of the analysis of the urban stormwater drainage systems capacity

In the research, the capacity of the sewer network was also examined. The water-carrying capacity data for the sewer network were obtained from the submitted permitting documentation. The runoff quantities assigned to the endpoints were compared with the water conveyance capacity of these endpoints' sewer systems. The sewer network and watershed areas were grouped, and the water yields for each corresponding watershed were aggregated along with the discharge capacities of the sewer networks covering those areas.

In the ME-Hydrograph model, we examined when the runoff of the combined watersheds reaches the drainage capacity of the corresponding sewer network. For individual watershed areas and watershed area groups, we calculated the maximum runoff values for various precipitation intensities and durations, as mentioned above *(Table 7).*

The data indicates the number of minutes for these flow values to reach the drainage capacity of the channel unit associated with the catchment area. In the vicinity of the area (Putnok), the maximum daily precipitation measured so far is 100 mm, so the occurrence of significantly larger rainfall is unlikely. The rightmost column shows the duration required to reach 100 mm of precipitation for the respective intensity values. It can be seen that the time required to reach 100 mm of rain is less than the time required to reach the threshold for each precipitation intensity. Accordingly, if rainfall exceeding the observations to date does not occur, the sewer network is capable of draining the runoff from the surrounding areas.

Conclusions

The results underline the importance of precise hydrological modelling to better understand and mitigate the impacts of intensive rainfall events.

By examining the methodologies and results of runoff models in other studies, it can generally be stated that, despite their wide applicability, the integration of remote sensing data (Courty, L. G. *et al.* 2017) and the opportunities provided by soil databases (Poortinga, A. *et al.* 2017; Shuli, W. *et al.* 2024) have not yet been incorporated into runoff models. Furthermore, in most cases, due to the absence of reliable precipitation forecasts, significant uncertainties are associated with the calculation of water discharge on so-called ultra-small hydrologically unexplored catchments. These uncertainties affect the determination of floodwave magnitudes impacting urban areas, as multiple sub-catchments may surround a settlement. In such cases, distributed hydrodynamic models are developed, and input data requirements are significantly increased (Hongping, Z. *et al.* 2021). Without these data, the assessment of sewer network loads caused by floodwaves, as well as the development of flood risk mapping methodologies, cannot be achieved.

The newly developed ME-Hydrograph model, alongside its GIS integration, has proven to be a reliable tool for evaluating surface runoff dynamics and assessing urban drainage system capacities. By incorporating detailed soil water absorption properties and calibrated boundary conditions, the model has achieved a high level of accuracy. To achieve the objectives of the study, several key actions were undertaken. First, boundary conditions were optimized using a combination of archive and field data, ensuring that the

*Table 7. Maximum water flow values for different rainfall scenarios**

Precipitation intensity, mm/h	Amount of time to reach				Number of minutes it takes for the rain to reach, 100 mm
	1. + 2.	3. + 4.	5.	6.	
	catchment limit value, min				
5	cannot reach	cannot reach	cannot reach	cannot reach	1200
10	800	cannot reach	810	cannot reach	600
15	530	cannot reach	540	520	400
20	420	420	410	390	300
25	330	330	330	310	240
30	280	280	280	270	200
40	210	210	210	210	150
50	170	170	170	170	120
Drainage capacity max., l/s	1194	754	2845	705	–

*Intensities and durations.

model accurately reflects local hydrological dynamics. Next, the land use and soil properties of the affected small watersheds were meticulously mapped, providing essential input data for runoff calculations. A general assessment of the soil and its infiltration characteristics across the watershed was also conducted, with infiltration rates estimated at representative points to capture spatial variability.

Building on this foundation, an existing runoff model, Stowe-Hydrograph, was refined and enhanced by incorporating the gathered data, culminating in the development of a new, more complex runoff model, ME-Hydrograph. This advanced model was designed to better simulate water movement and retention dynamics within the target area. Finally, the models were compared, and the load capacity of the existing drainage system was assessed based on the permitting plan, offering valuable insights into the system's ability to manage runoff under varying conditions. The similarity of the percentages of runoff and retained water confirms that the GIS application developed by ME effectively models water runoff by accurately considering the soil's water absorption capacity. This results in reliable hydrographs that closely reflect real-world conditions. The consistency of the outcomes demonstrates the robustness of the method, highlighting its ability to produce dependable and reproducible results across varying scenarios.

During the drainage system load capacity assessment, it was determined that, considering the maximum precipitation load, the urban sewer network of Sajószentpéter is capable of draining the surface runoff from the surrounding catchment areas. This has been confirmed based on several different precipitation event scenarios. However, several factors (e.g. implementation of additional surface, land use properties and consideration of linear infrastructure) have not yet been included in the model, which will be subjects of future research.

The future of the ME-Hydrograph is primarily characterized by the integration of machine learning algorithms. However, due to the inherent non-linear nature of these methods, their application is possible only when supported by robust theoretical foundations (Jehanzaib, M. *et al.* 2022). While the increased data demands associated with soil surface characteristics pose challenges, the implementation of NDVI and other indices has initiated this progression, offering a potential framework to guide future research efforts (Gupta, A. *et al.* 2024; Shuli, W. *et al.* 2024). In this context, significant potential lies in the integration and connection of the region's digital soil map (E-Soter soil database) with the research, enabling its application to larger-scale catchments (Dobos, E. *et al.* 2007). Nevertheless, in parallel with the development of runoff modelling, the enhancement of flood risk mapping methodologies remains essential to ensure proper validation.

***Acknowledgement*:** We would like to take this opportunity to highlight and express our gratitude for the development and extension of the runoff model in Python by Péter Vadnai, as well as for the support and contributions he provided to the project. The research was carried out with funding by the 2020-1.1.2-PIACI-KFI: Support for Market-Driven Research, Development, and Innovation Projects – Development of an ICT Platform for Supporting Soil Information-Driven Agriculture for Managing and Optimizing Agricultural Production and Monitoring the Effects on the Soil System. Also funded by the RRF-2.3.1-21-2022-00014 Climate Change Multidisciplinary National Laboratory for Climate Change, and within the framework of the Széchenyi Plan Plus program with the support of the RRF 2.3.1 21 2022 00008 project.

REFERENCES

Agroszkin, I.I., Dmitrijev, G.T. and Pikalov, F.I. 1952. *Hidraulika* (Hydraulics). Budapest, Tankönyvkiadó.

Balatonyi, L. 2015. *Árvízhozam előrejelzés optimalizálása középhegységi és dombvidéki kisvízgyűjtőkre* (Optimization of flood discharge forecasting for small catchments in hilly and mountainous regions). PhD thesis. Pécs, Pécsi Tudományegyetem Természettudományi Kar, Földtudományok Doktori Iskola.

Baros, Z., Homoki, E. and Juhász, Cs. 2001. *Bányászati hatások vizsgálata a Tardona-patak vízgyűjtőjén* (Investigation of mining impacts on the Tardona Stream catchment). Paper for National Scientific

Students' Associations (OTDK) Conference. Debrecen, Debreceni Egyetem Ásvány- és Földtani Tanszék.

Bihari, Z., Babolcsai, Gy., Bartholy, J., Ferenczi, Z., Gerhátné, K.J., Haszpra, L., Homokiné, U.K., Kovács, T., Lakatos, M., Németh, Á., Pongrácz, R., Putsay, M., Szabó, P. and Szépszó, G. 2018. Climate. In *National Atlas of Hungary, Vol. 2: Natural Environment*. Editor-in-Chief: Kocsis, K., Budapest, MTA CSFK Geographical Institute, 58–69. https://nationalatlas.hu

Chow, V.T. 1959. O*pen-Channel Hydraulics*. New York, McGraw-Hill.

Courty, L.G., Pedrozo-Acuña, A. and Bates, P.D. 2017. Itzï (version 17.1): An open-source, distributed GIS model for dynamic flood simulation. *Geoscientific Model Development* 10. (4): 1835–1847. https://doi.org/10.5194/gmd-10-1835-2017

Czigány, Sz., Pirkhoffer, E. and Geresdi, I. 2009. Environmental impacts of flash floods in Hungary. In *Flood Risk Management: Research and Practice.* Eds.: Samuels, P., Huntington, S., Allsop, W. and Harrop, J., London, Taylor & Francis Group, 1439–1447. https://doi.org/10.1201/9780203883020.ch169

Dobos, E., Daroussin, J. and Montanarella, L. 2007. A quantitative procedure for building physiographic units for the European SOTER database. In *Digital Terrain Modelling. Lecture Notes in Geoinformation and Cartography*. Eds.: Peckham, R. and Jordan, Gy., Berlin–Heidelberg, Springer, 227–258. https://doi.org/10.1007/978-3-540-36731-4_10

Dövényi, Z. (ed.) 2010. *Magyarország kistájainak katasztere* (Inventory of microregions in Hungary). Budapest, MTA Földrajztudományi Kutatóintézet.

Du, J., Fan, Zj. and Pu, J. 2020. Comparative study on flash flood hazard assessment for Nam Ou River Basin, Lao PDR. *Natural Hazards* 102. (3): 1393–1417. https://doi.org/10.1007/s11069-020-03972-3

Goda, Z. 2019. A villámárvizek meteorológiai háttere (Meteorological background of flash floods). In *Országos Települési Csapadékvíz-gazdálkodási Konferencia Tanulmányai.* Ed.: Bíró, T., Budapest, Dialóg Campus Kiadó, 149–158.

Guo, L., He, B., Ma, M., Chang, Q., Li, Q., Zhang, K. and Hong, Y. 2018. A comprehensive flash flood defense system in China: Overview, achievements, and outlook. *Natural Hazards* 92. 727–740. https://doi.org/10.1007/s11069-018-3221-3

Gupta, A., Hantush, M.M., Govindaraju, R.S. and Beven, K. 2024. Evaluation of hydrological models at gauged and ungauged basins using machine learning-based limits-of-acceptability and hydrological signatures. *Journal of Hydrology* 641. 131774. https://doi.org/10.1016/j.jhydrol.2024.131774

Harangi, Sz. 2001. Neogene to Quaternary volcanism of the Carpathian-Pannonian Region – A review. *Acta Geologica Hungarica* 44. (2–3): 223–258.

Hongping, Z., Weiming, W., Chunhong, H., Changwei, H., Min, L., Xiaoli, H. and Shu, L. 2021. A distributed hydrodynamic model for urban storm flood risk assessment. *Journal of Hydrology* 600. 126513. https://doi.org/10.1016/j.jhydrol.2021.126513

Jakab, G., Bíró, T., Kovács, Z., Papp, Á., Sarawut, N., Szalai, Z., Madarász, B. and Szabó, Sz. 2019. Spatial analysis of changes and anomalies of intense rainfalls in Hungary. *Hungarian Geographical Bulletin* 68. (3): 241–253. https://doi.org/10.15201/hungeobull.68.3.3

Jehanzaib, M., Ajmal, M., Achite, M. and Kim, T.-W. 2022. Comprehensive review: Advancements in rainfall-runoff, modelling for flood mitigation. *Climate* 10. (10): 147. https://doi.org/10.3390/cli10100147

Kontur, I., Koris, K. and Winter, J. 2003. *Hidrológiai számítások* (Hydrological calculations). Budapest, Linográf Kft.

Koris, K. 2021. The new Hungarian empirical flood calculation guide has been completed, the OVF-2020. *Hungarian Journal of Hydrology* 101. 13–19.

Kozák, M. and Püspöki, Z. 1995. Correlative relationship between denudational periods and sedimentation in the forelands of the Bükk Mountains (NE Hungary). In *Proceedings of CBGA XV. Congress*. Athens, CBGA, 340–345.

Kozák, M., Püspöki, Z., Piros, O. and László, A. 1998. The structural position of the Bükk Mountains based on tectono- and pebble stratigraphic analyses. In *Proceedings of CBGA XVI. Congress*. Vienna, CBGA, 303.

Maidment, D.R., Olivera, F., Calver, A., Eatherall, A. and Fratzek, W. 1996. Unit hydrograph derived from a spatially distributed velocity field. *Hydrological Processes* 10. (6): 831–844. https://doi.org/djxpvm

Mikes, M.Z., Pieczka, I. and Dezső, Zs. 2024. Characteristics and observed seasonal changes in Cold Air Outbreaks in Hungary using station data (1901–2020). *Hungarian Geographical Bulletin* 73. (2): 115–130. https://doi.org/10.15201/hungeobull.73.2.1

Pandey, K., Verma, L. and Verma, A.K. 2011. L-stable Simpson's 3/8 rule and Burgers' equation. *Applied Mathematics and Computation* 218. (4): 1342–1352. https://doi.org/10.1016/j.amc.2011.06.017

Péczely, Gy. 2006. *Éghajlattan* (Climatology). Budapest, Nemzeti Tankönyvkiadó.

Pelikán, P. 2002. Földtani felépítés, rétegtani áttekintés (Geological structure, stratigraphic overview). In *A Bükki Nemzeti Park*. Ed.: Baráz, Cs., Eger, Bükki Nemzeti Park Igazgatóság, 23–49.

Pilgrim, D.H. 1976. Travel times and nonlinearity of flood runoff from tracer measurements on a small watershed. *Water Resources Research* 12. (3): 487–496. https://doi.org/10.1029/WR012i003p00487

Pirkhoffer, E., Czigány, Sz., Hegedűs, P., Balatonyi, L. and Lóczy, D. 2013. Lefolyási viszonyok talajszempontú analízise ultra-kisméretű vízgyűjtőkön (Analysis of runoff conditions from a soil perspec-

tive in ultra-small watersheds). *Tájökológiai Lapok* 11. (1): 105–123. https://doi.org/10.56617/tl.3737

Poortinga, A., Bastiaanssen, W., Simons, G., Saah, D., Senay, G., Fenn, M., Bean, B. and Kadyszewski, J. 2017. A self-calibrating runoff and streamflow remote sensing model for ungauged basins using open-access earth observation data. *Remote Sensing* 9. (1): 86. https://doi.org/10.3390/rs9010086

Ramos Filho, G.M., Coelho, V.H.R., Freitas, E., Xuan, Y. and Almeida, C. 2021. An improved rainfall-threshold approach for robust prediction and warning of flood and flash flood hazards. *Natural Hazards* 105. (3): 2409–2429. https://doi.org/10.1007/s11069-020-04405-x

Shuli, W., Wei, W. and Guizhang, Z. 2024. A novel deep learning rainfall-runoff model based on Transformer combined with base flow separation. *Hydrology Research* 55. (5): 576–594. https://doi.org/10.2166/nh.2024.035

Sütő, L. 2001. A felszín alatti bányászat domborzatra gyakorolt hatásai a Kelet-Borsodi-szénmedencében (Effects of subsurface mining on topography in the Eastern Borsod Coal Basin). In *Magyar Földrajzi Konferencia: A földrajz eredményei az új évezred küszöbén*. Ed.: Dormány, G.I., Szeged, SZTE, 1–20.

Szirmai, O. and Czóbel, Sz. 2008. A Tardonai-dombság egyik vonulatának aktuális vegetációtérképe (Current vegetation map of a ridge of the Tardona Hills). In *Aktuális Flóra- és Vegetációkutatás a Kárpát-medencében VIII.* Gödöllő, 29 February – 2 March 2008. Summaries of the presentations of the conference. *Kitaibelia* 13. (1): 190.

Várallyay, Gy. and Fórizs, J. 1966. A helyszíni talajfelvételezés módszertana (Methodology of in situ soil survey). In *A genetikus üzemi talajtérképezés módszerkönyve*. Ed.: Szabolcs, I., Budapest, Táncsics Könyvkiadó, 19–164.

Víg, B., Fábián, Sz.Á., Czigány, Sz., Pirkhoffer, E., Halmai, Á., Kovács, I.P., Varga, G., Dezső, J., Nagy, G. and Lóczy, D. 2022. Morphometric analysis of low mountains for mapping flash flood susceptibility in headwaters. *Natural Hazards* 114. 3235–3254. https://doi.org/10.21203/rs.3.rs-1318911/v1

Other source:

arcgis.com: STOWE Hydrographdeveloped by Esri's Learn Team, Predict floods with unit hydrographs. Available at www.learn.arcgis.com/en/projects/predict-floods-with-unit-hydrographs